Available online at www.sciencedirect.com

SCIENCE DIRECT®

Coastal Engineering 51 (2004) 1163–1184

Coastal Engineering
An International Journal for Coastal, Harbour and Offshore Engineers

www.elsevier.com/locate/coastaleng

Flow tunnel measurements of velocities and sand flux in oscillatory sheet flow for well-sorted and graded sands

Tom O'Donoghue*, Scott Wright[1]

University of Aberdeen, Department of Engineering, King's College, Aberdeen AB24 UE, Scotland

Received 1 April 2004; received in revised form 11 August 2004; accepted 12 August 2004
Available online 14 October 2004

Abstract

Oscillatory flow tunnel measurements of velocities and fluxes for sands in oscillatory sheet flow conditions are presented. The experiments involved a range of well-sorted and graded sands in two asymmetric flows. Velocities were measured using an ultrasonic velocity profiler (UVP) capable of measuring deep within the sheet flow layer. Velocity profiles are found to be similar for the same flow but different sand beds and display expected features of oscillatory boundary layer flow. The near-bed velocity leads the main flow velocity by approximately 21° and a small offshore-directed current is generated near the bed. Measures of the boundary layer thickness are in good agreement with those predicted using an equation formulated for the boundary layer thickness over fixed beds. Velocity data have been combined with concentration data to produce time-dependent sand flux profiles covering the sheet flow and suspension regions. There are fundamental differences in the transport processes of sands of different size and grading, caused by unsteady effects which dominate in the case of fine sand and are largely absent in the case of coarse sand. (1) Time-averaged flux is onshore-directed (positive) in the case of coarse sand and is confined to a region immediately above the bed; in contrast, time-averaged flux in the case of fine sand extends high above the bed, is offshore-directed (negative) in the sheet flow layer and becomes onshore-directed in the suspension layer. (2) Net transport in the case of coarse sand is directed onshore. As the percentage of fine sand in the bed increases, offshore transport becomes increasingly dominant as the percentage of fine sand increases. (3) Net transport in the suspension layer is onshore while net transport in the sheet-flow layer may be onshore or offshore depending on sand size and grading.

Keywords: Sediment transport; Sheet flow; Graded sediments; Sand flux; Flow tunnel experiments; Oscillatory flow; Boundary layer

1. Introduction

The response of a sandy seabed to waves depends on the sand size and the near-bed oscillatory flow generated by the waves. When flow velocities are high the sand transport takes place within a water–sediment mix moving over a flat, ripple-free bed. This

* Corresponding author. Tel.: +44 1224 272508; fax: +44 1224 272497.
E-mail address: t.o'Donoghue@eng.abdn.ac.uk (T. O'Donoghue).
[1] Former Research Assistant, University of Aberdeen. Currently with JP Jenny Caledonia Ltd., Aberdeen.

0378-3839/$ - see front matter © 2004 Published by Elsevier B.V.
doi:10.1016/j.coastaleng.2004.08.001

transport regime is called "sheet flow". Because of the high velocities and the high concentrations of sand moving within the sheet flow layer, high transport rates are associated with the sheet flow regime and it is important to develop well-founded models for predicting these transport rates. The development of reliable sheet flow transport models has therefore been the focus of much research effort. Existing models include two-phase flow models (e.g. Dong and Zhang, 2002; Kaczmarek and Ostrowski, 2002), which aim to describe the detailed fluid–sediment interactions in the sheet flow layer, single phase models based on solution of the momentum equation for water flow and the advection–diffusion equation for sediment concentration (e.g. Li and Davies, 1996; Ribberink and Al-Salem, 1995) and empirical models that are largely based on experimental data (Bailard, 1981; Ribberink, 1998). There has also been much interest in so-called 'semi-empirical' models, which aim to explicitly account for specific physical processes through parameterisations based on experimental data and physical argument. Examples of the latter include the sand transport models of Dohmen-Janssen et al. (2002) and Dibajnia and Watanabe (1991), which take explicit account of the unsteady phase lag effects associated with fine sands.

Confidence in predictive models depends on good agreement between predicted and measured transport rates for well defined conditions and, for physics-based models, good agreement between measured and predicted processes such as time-dependent concentrations, velocities and sediment fluxes. Detailed measurements of wave-generated sheet flow processes are not yet technically feasible in the field. The most useful measurements, free from scale effects, have come from experiments with sand in large oscillatory flow tunnels and a few experiments in large ('full-scale') wave flumes (see Wright, 2002; Dohmen-Janssen, 1999 for reviews). These experiments have yielded good data for transport rates and sheet flow concentrations but are very limited with respect to sheet flow velocities and, therefore, sand fluxes. This has been due to the limitations of existing equipment for velocity measurement in the presence of high sand concentrations in the sheet flow layer.

The present paper is based on a programme of sheet flow experiments conducted in a large oscillatory flow tunnel. The experiments covered a range of well-sorted and mixed sands in full-scale oscillatory flow conditions. Ultrasonic velocity profiling (UVP) equipment was available for some of the experiments and was found to be capable of measuring velocities deep within the sheet flow layer. The detailed results for sheet flow concentration are presented elsewhere (O'Donoghue and Wright, 2004). In the present paper, we present velocity measurements and combine them with concentration measurements to produce time-varying sand flux profiles. The flux profiles give insight into the fundamental transport processes, including the effects of sand size and grading. The paper presents integrated flux results to examine onshore, offshore and net sand transport rates, transport rates in the sheet flow and suspension layers and intra-wave transport in the sheet flow layer.

2. Background

Oscillatory sheet flow conditions prevail when the wave-generated bed shear stress is high and the maximum value of the Shields parameter exceeds approximately 0.8 (Nielsen, 1992). Time-varying Shields parameter is defined as

$$\theta(t) = \frac{\tau_o(t)}{\rho(s-1)gd} = \frac{\frac{1}{2}f_w u_0^2(t)}{(s-1)gd} \tag{1}$$

and the maximum value of the Shields parameter corresponds to the maximum flow velocity, i.e.

$$\theta_m = \frac{\tau_{om}}{\rho(s-1)gd} = \frac{\frac{1}{2}f_w u_m^2}{(s-1)gd} \tag{2}$$

In Eqs. (1) and (2): $\tau_o(t)$ is bed shear stress; $u_o(t)$ is the wave-generated, near-bed, horizontal flow velocity above the bottom boundary layer (the main or outer flow velocity); u_m is the maximum outer flow velocity; s is sediment specific gravity (s=2.65 for sand); g is acceleration due to gravity; d is sediment size (usually the d_{50} in the case of a sand bed); and f_w is the wave friction factor. The Jonsson (1966) or Swart (1974) formulae are often used to calculate f_w for sheet flow conditions. In these formulae, f_w is a function of the ratio of flow orbital amplitude, A, to bed roughness, k, with k typically taken as 2.5d. However, the appropriateness of such formulae to sheet flow conditions, for which a layer of high concentration sediment is present above the undisturbed bed, is open to question. For example, Wilson (1989) argues that f_w for sheet flow conditions is independent of d and depends on A and the oscillatory flow period, T.

Fig. 1 provides a definition sketch for sheet flow. It illustrates vertical profiles of concentration, velocity and sediment flux at a particular phase in the oscillatory flow cycle. z measures elevation with z positive upwards and z=0 corresponds to the no-flow bed level. The elevation of the undisturbed bed varies during the flow in response to the varying bed shear stress. The instantaneous distance from the no-flow bed level to the undisturbed bed is the erosion depth, $\delta_e(t)$. Erosion depth depends primarily on applied bed shear stress and empirical equations for maximum erosion depth, δ_{em}, take the form

$$\frac{\delta_{em}}{d_{50}} = C_1\theta_m + C_2 \tag{3}$$

where C_1 and C_2 are empirical constants. (C_1,C_2) values of (8.5,0), (3,0) and (8.3,−5.5) have been proposed by Asano (1992), Zala-Flores and Sleath (for sand, 1998) and O'Donoghue and Wright (2004), respectively. Erosion depths are small for typical sand sizes in wave-generated sheet flow conditions. For example, Eq. (3), with (C_1,C_2)=(8.3,−5.5) gives δ_{em} less than 5 mm for typical sands in oscillatory flow conditions with a maximum flow velocity of 1.5 m/s.

In Fig. 1, c' is concentration normalised with respect to sediment concentration in the undisturbed bed, $c_o \approx 1650$ g/l. At $z=-\delta_e(t)$, $c'(t)=1.0$ and c' decreases with increasing z. In the sheet flow layer, sediment concentration decreases very rapidly with height. The sheet flow layer thickness, $\delta_s(t)$, covers the region from $z=-\delta_e(t)$ to an upper limit where intergranular stresses are negligible. Different researchers have used different quantitative definitions for the upper boundary of the sheet flow layer. In Fig. 1, we adopt Dohmen-Janssen's (1999) suggestion that the upper boundary be defined as the elevation in the flow where the volumetric concentration is 8% (i.e. c'=0.13), the argument being that at this concentration average grain spacing is approximately one grain diameter and grain-to-grain interactions are therefore negligible. Sheet flow layer thickness tends to be small, especially for coarser sands. For example, in oscillatory flow with a maximum velocity of 1.5 m/s, the upper boundary of the sheet flow layer for coarse sand typically lies within a few millimetres above z=0 so that the maximum sheet flow layer thickness, δ_{sm}, is of the order of 5 mm; for fine sand, δ_{sm} is of the order of 1–2 cm for the same flow magnitude. Above $z=\delta_s(t)-\delta_e(t)$ is the suspension layer where the concentration profile is determined by turbulent diffusion processes. Measurements of suspended sediment concentrations during various sheet flow experiments carried out in the LOWT at Delft Hydraulics indicate that the time-averaged concentration profile in the suspension layer may be described by a power law with exponent depending on bed sand size and grading (Ribberink and Al-Salem, 1994; Ribberink and Chen, 1993; Katopodi et al., 1994; Dohmen-Janssen, 1999).

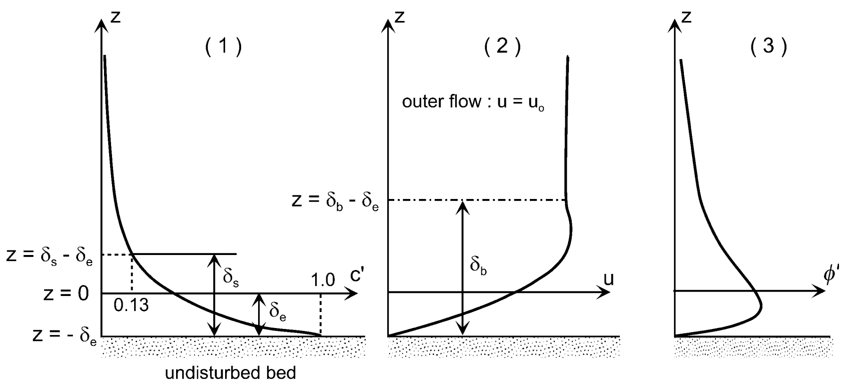

Fig. 1. Definition sketch.

The second graph in Fig. 1 illustrates the instantaneous velocity profile. The bottom boundary layer extends from $z=-\delta_e(t)$ to $z=\delta_b(t)-\delta_e(t)$, where $\delta_b(t)$ is the instantaneous boundary layer thickness as shown. Within the boundary layer, u increases from $u=0$ at $z=-\delta_e(t)$ to $u=u_o(t)$ at $z=\delta_b(t)-\delta_e(t)$, but u may exhibit a local maximum within the boundary layer (the velocity "overshoot") depending on the phase. Detailed velocity measurements have been made of oscillatory boundary layer flow over rough, fixed beds (Sleath, 1987; Jensen et al., 1989) and the boundary layer thickness has been shown to depend on relative roughness, A/k, with k being of the order of the (fixed) sediment size. For sheet flow however, the presence of high concentrations of moving sediment increases energy dissipation within the boundary layer and the roughness is often considered to be a multiple of the sheet flow layer thickness, δ_s, rather than the sediment size (e.g. Grant and Madsen, 1982; Wilson, 1989). Estimates of k for sheet flow vary widely (Dohmen-Janssen, 1999): typical values are a factor of 10–100 times the fixed bed k value. Based on Sleath's formula for boundary layer thickness (Sleath, 1987) in which δ_b is proportional to $k^{0.3}$, δ_b for sheet flow may therefore be expected to be two to four times that of a fixed bed. However, very few detailed measurements exist of sheet flow velocities for natural sands in oscillatory flows with which to better define the roughness and the boundary layer thickness.

The third graph in Fig. 1 illustrates the instantaneous flux profile given by $\phi'(z,t)=c'(z,t)u(z,t)$. To date, very few measurements of time-varying flux have been reported for sheet flow conditions, mainly because of difficulties associated with velocity measurement in the sheet flow layer. The focus of the present paper is on new measurements of sheet flow sand flux. Time-varying flux profiles and integrated fluxes are presented, which illustrate important aspects of the processes determining net sand transport.

3. Experimental set-up

The experiments were conducted in Aberdeen University's oscillatory flow tunnel (AOFT). The tunnel has an overall length of 16 m with a 10 m long, glass-sided rectangular test section, 0.75 m high and 0.3 m wide. The experiments were conducted with a 250-mm deep sand bed occupying the central 6 m of the test section, bound at either end by marine plywood ramps, fixed to the tunnel floor and sealed to the tunnel sides. The set-up is illustrated and described more fully in O'Donoghue and Wright (2004). The present paper is based on the measurements of net sand transport rate and concentrations and velocities in a region extending from the erosion depth to approximately 150 mm above the initial bed level.

3.1. Concentration measurement

Concentrations in the sheet flow layer were measured using conductivity concentration probes (CCMs), similar to those used in experiments carried out in the LOWT at Delft Hydraulics (see, for example, Ribberink and Al-Salem, 1995). Given the high concentration gradients within the sheet flow layer and the tendency for the bed level to change by a few millimeters during the course of an experiment, special probe deployment and data interpretation methods were used to determine the exact elevation of each concentration measurement. Details and results are presented in O'Donoghue and Wright (2004).

CCMs measure high concentrations and cannot be used to measure the low sand concentrations present in the suspension layer. Concentrations in the suspension layer were measured by suction sampling. Eight suction samplers were deployed, equally spaced logarithmically over the initial, no-flow bed level at elevations in the range $5 \leq z \leq 150$ mm, as illustrated in Fig. 2. The nozzle diameter of each sampler was 3.16 mm and the samplers were oriented transverse to the flow in accordance with Bosman et al.'s (1987) recommendations for concentration measurement by suction sampling. The samplers supplied sediment-laden flow to a carousel-type collector similar in concept to that used by Staub et al. (1996), but with the important difference that peristaltic pumps were used here to maintain constant discharge from each sampler. The collector consists of eight rotating carousels, one for each sampler in the tunnel, with each carousel consisting of 20 bottles (Fig. 3). A dc motor and speed control unit provide power and precise speed control. When the carousels are rotating

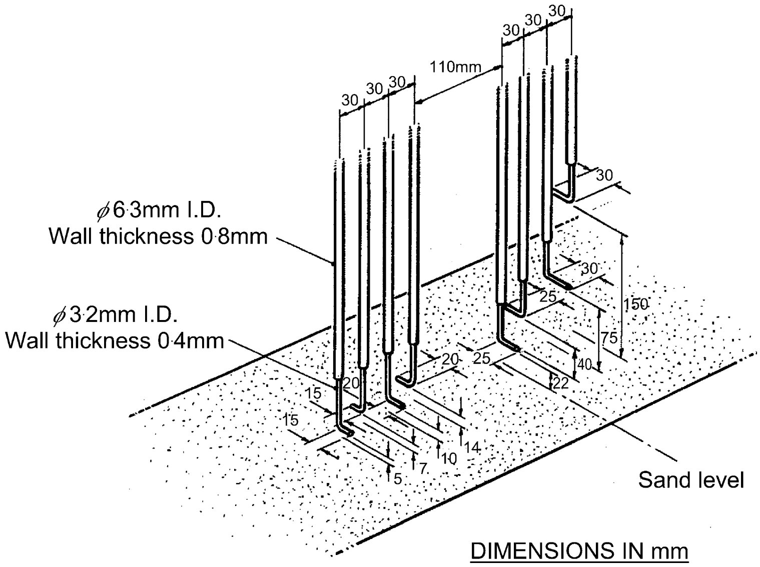

Fig. 2. Suction sampler deployment.

with the same frequency as the oscillatory flow in the tunnel, suspended sand corresponding to a particular 1/20th of the oscillatory period is collected in each bottle. Sampling was typically carried out over 25 flow cycles. The phase of the concentration measurement was obtained by starting and stopping sampling at a known phase in the wave cycle, noting the first bottle sampled to and accounting for the time lag between the sediment-laden water entering the sampler in the tunnel and discharging into the bottles on the carousel.

The suction samplers produced a significant lowering of the mean bed level (in the range 10–30 mm) in the vicinity of the samplers during the course of the experiment. (For this reason, separate runs of the experiments were carried out for the suction measure-

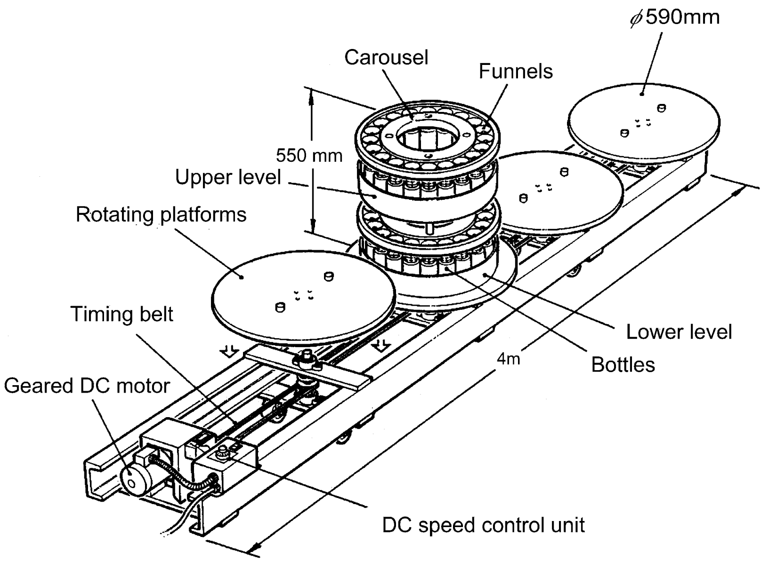

Fig. 3. Carousel collector.

ments and the CCM measurements with the samplers removed from the tunnel during the CCM measurements.) To account for the bed level drop during the suction measurements, the sampler positions were taken as the mean of their heights at the start and end of the test. As a result, the height of the lowest suction concentration measurement was generally in the range 7.5–17.5 mm above the initial, no-flow bed level. The CCM concentration measurements extend from the erosion depth upwards through the sheet flow layer. Good CCM measures of concentration are only possible where concentration is relatively high. The CCM measurements are robust for c>160 g/l (i.e. c'>0.1), which, for the test conditions used here, typically corresponds to z less than approximately 5 mm. There is therefore a gap of the order of 10 mm in the measured concentration profile between the CCM-measured concentrations in the sheet flow layer and the suction-measured concentrations in the suspension layer. Of course, this gap is subsequently present in the flux profiles and, as discussed later, creates some difficulty in integrating flux profiles for transport rates.

3.2. Velocity measurement

Measurements of sheet flow velocities in oscillatory flows are relatively rare because of the difficulties associated with velocity measurement within high sediment concentration flows. Horikawa et al. (1982) used a photographic technique and a frame-by-frame analysis to measure sheet flow velocities in flow tunnel experiments with sand and plastic particles and succeeded in obtaining velocity measurements down to about 2 mm above the no-flow bed level. Asano (1995) used a similar method for experiments with light plastic particles. Dick and Sleath (1991, 1992) used LDA (laser Doppler anemometry) in sheet flow experiments with acrylic and pvc particles and Zala Flores and Sleath (1998) used the same method in experiments with 0.41-mm sand. Ribberink and Al-Salem (1995) used LDA for oscillatory flows over a 0.21-mm sand bed and found that sheet flow velocity measurements were not reliable below about 20 mm above the no-flow bed level. McLean et al. (2001) measured sheet flow velocities in large flow tunnel experiments with 0.13- and 0.32-mm sands by cross-correlating concentration measurements from two CCM probes spaced 15–20 mm apart in the streamwise direction. Dohmen-Janssen and Hanes (2002) used the same method for experiments with 0.24-mm sand in a very large wave flume.

Despite these efforts, the quantity of good quality sheet flow velocity data is small because of the difficulties and limitations associated with the methods and equipment used. The main practical difficulty has been the presence of very high sand concentrations, which prevents measurement of velocity deep in the sheet flow layer using standard laser Doppler (LDA) or acoustic Doppler (ADV) equipment. This difficulty has been avoided in the present study by using an ultrasonic velocity profiler (UVP, manufactured by METFLOW) for the velocity measurements. The UVP is similar in principle to acoustic Doppler velocimeters (ADVs) commonly used in hydraulics experiments, in that measurement is based on pulsed ultrasound echography together with a detection of Doppler shift frequency. A fundamental difference however is that the acoustic frequency in the case of the UVP is much lower than the 10 MHz ADV frequency, enabling the UVP to measure in flows with much higher sediment concentration. A second big advantage of the UVP is that it simultaneously measures velocities at 128 locations along the beam axis, thereby measuring the instantaneous velocity "profile". The profile length covered by the 128 locations is variable up to 750 mm. Profile length and acoustic frequency determine the measurement volume and the maximum measurable velocity. For example, for a 2 MHz transducer, the maximum measurable velocity in the direction of the ultrasound beam is 0.18 m/s for a profile length of 750 mm and 1.32 m/s for a profile length of 100 mm; if the UVP is at, say, 45° to the flow direction, then the corresponding maximum flow velocities are 0.25 and 1.87 m/s, respectively. Depending on measurement parameters, 30–200 profiles can be measured and saved every second.

The velocities presented here were measured using 2 MHz transducers set to measure over a distance of approximately 100 mm along the beam axis. The probe was fitted within a stainless steel mounting that screwed into the end of a 25-mm diameter, thick-walled stainless steel tube (Fig. 4). The complete unit entered the tunnel through the roof via a large plastic block that anchored the tube at a particular angle to

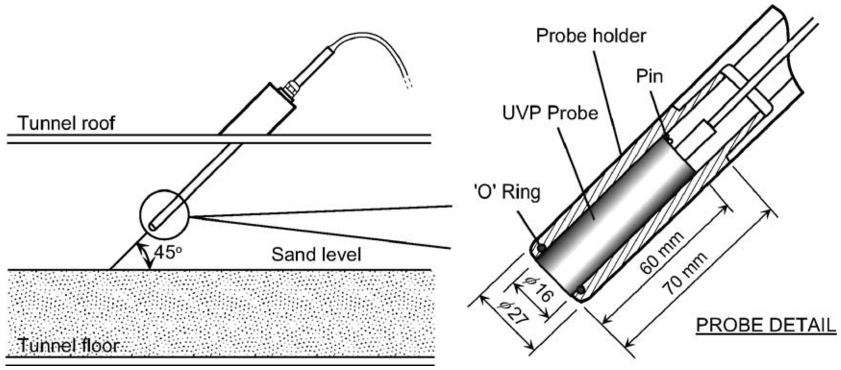

Fig. 4. UVP deployment.

the tunnel's main flow. Trials were carried out using different angled blocks and very similar results were obtained for different probe angles. Results presented in this paper were obtained with the probe at 45° to the flow. With this set-up, the measurement volume is 0.74 mm along the beam axis giving a vertical resolution in the measurements of 0.56 mm (i.e. 100 sin 45°/127); the velocity resolution is 10.4 mm/s along the beam axis. The mounting tube was a tight fit in the plastic block but it could be moved up and down in order to set the probe head at the required distance from the sand bed. Velocity measurement started after two flow cycles following tunnel start-up and continued for a further 10 cycles sampling at 20 Hz. Velocity profiles at different phases of the flow cycle are based on phase-averages over the 10 flow cycles. Each experiment was repeated approximately eight times and agreement between measured profiles from different runs was very good.

3.3. Net sand transport measurement

Sediment transport was measured by applying the mass conservation principle to the measured pre- and post-test bed profiles with the masses of sand collected from the two ends of the test section. A flat, horizontal bed with vertical and horizontal homogeneity was first prepared and the pre-test bed profile measured; flow was started and allowed to run for 20 cycles; the post-test bed profile was measured and all sand carried off the onshore and offshore ends of the test section was collected; the collected sand was oven-dried and weighed to give the "offshore" and "onshore" dry masses of collected sand. Bed profiling was carried out using a laser displacement sensor mounted on a computer-controlled x–y positioning frame. The sensor has a spot diameter of 1 mm and a vertical resolution of 50 μm. Measurements were made of bed elevation at 2-mm intervals along five longitudinal profiles at 50-mm spacing across the tunnel width. The 20-cycle test duration was chosen because it was sufficiently long to produce significant sand transport while being sufficiently short to avoid major loss of sand from the test bed and significant changes in bed composition caused by selective transport processes. One experiment was repeated with a 40-cycle duration (X4A5010) to test the sensitivity of the transport measurement to test duration: the transport results obtained from the two experiments were within 15% of each other suggesting that effects of sand loss and bed composition changes are very small within a 20-cycle measurement period.

Estimates of net sand transport were obtained in two ways. For the first method, the time-averaged sand transport rate as a function of distance along the test section was calculated using mass conservation principles applied to the masses of collected sand and the pre- and post-test bed profiles. Net transport is then taken as the transport rate obtained midway along the test section, where, ideally, the transport is unaffected by the ends and is near constant. The second method involves calculation of the net transport directly from the masses of sand collected from the ends of the test bed (Dibajnia and Watanabe, 1998). Essentially, this method is based on the assumption that the mass of sand collected at the onshore end represents the onshore (positive) transport and the mass of sand collected at the offshore end represents the offshore (negative) transport. End effects associated with the limited length of test bed affect both types of measurement of the net transport rate and it is difficult to quantify the accuracy of the transport measurement caused by these end effects. For the present experiments, the transport rate estimates obtained using the two methods were found to be within 30% of each other for all experiments except 2 for which the differences were 50% and 80%. For most of the experiments, a central region of near constant transport tended not to occur. Instead, the region of constant transport was located either towards the onshore end of the test section for experiments with net onshore transport or towards the offshore end of the test section for experiments with net offshore transport and net transport rates in these constant regions were in very good agreement with the transport rates determined using the second method. For this reason, net transport rates obtained using the second method have been used in what follows.

4. Range of experiments

The complete experimental programme involved seven sands tested in a range of sinusoidal and asymmetric oscillatory flow conditions. The present paper focuses on the asymmetric flow experiments because these produce a net transport. These experiments involved six sands, the properties of which are presented in Table 1. They comprise three well-sorted sands—"fine", "medium" and "coarse" with d_{50} values of 0.15, 0.28 and 0.51 mm, respectively—and three mixed sands, each consisting of different proportions of the three well-sorted sands. Table 1 contains two values for each sand size: one is the size obtained using a laser diffraction particle size analyser (Malvern) and the bracketed value is the size obtained using sieve analysis. The sizes differ slightly because the particle size analyser measures a "diameter" which corresponds to the diameter of a sphere of equivalent volume as the particle being measured, whilst sieve analysis measures the smaller "diameter" of the particle. The sands were tested in a range of asymmetric flow conditions, of same form as the near-bed horizontal flow produced by second order Stokes waves, i.e. the main flow velocity is defined by

Table 1
Size characteristics of the sands used for the experiments (sieve values in brackets)

Name	Mix %F–%M–%C	d_{10} (mm)	d_{50} (mm)	d_{90} (mm)
Fine (F)	100–0–0	0.10 (0.10)	0.15 (0.13)	0.23 (0.17)
Medium (M)	0–100–0	0.17 (0.17)	0.28 (0.27)	0.45 (0.39)
Coarse (C)	0–0–100	0.36 (0.35)	0.51 (0.46)	0.67 (0.58)
Mix1 (X1)	60–30–10	0.11 (0.10)	0.19 (0.15)	0.45 (0.40)
Mix2 (X2)	20–60–20	0.14 (0.12)	0.28 (0.27)	0.53 (0.47)
Mix4 (X4)	50–0–50	0.11 (0.10)	0.28 (0.26)	0.61 (0.53)

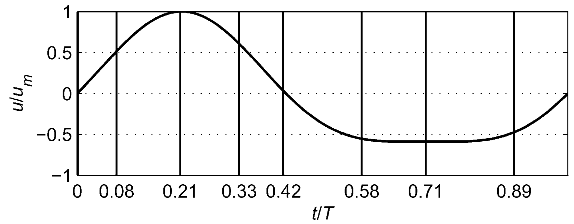

Fig. 5. Main flow velocity; thick lines indicate phases for which results are presented in other figures.

$$u(t) = u_1 \ \sin \ \omega t - u_2 \ \cos \ 2\omega t \tag{4}$$

where $\omega=2\pi/T$ and u_1 and u_2 determine the magnitude and asymmetry, as, of the main flow velocity. Asymmetry is defined here as

$$as = \frac{u_\mathrm{m}}{u_\mathrm{m} - u_\mathrm{min}} \tag{5}$$

where u_m is the maximum positive (onshore) outer flow velocity and u_min is the maximum negative velocity. For these experiments, u_1 and u_2 were chosen so that as=0.63 for all flows. Fig. 5 shows the form of the velocity time-history and also indicates phases in the flow cycle for which velocity and flux results are presented later in the paper.

Table 2 summarises the test conditions. The experiments involved the six sands in two flows, one with T=5 s and one with T=7.5 s. The values of maximum Shields parameter, θ_m, shown in the table are based on u_m and the Malvern-measured d_{50} of the sands. The θ_m values are based on friction factor estimated using Swart (1974). (θ_m values based on Swart are very similar to θ_m based on Wilson et al., 1995, except in the case of the fine sand for which f_w from Swart is approximately 0.8 times f_w from Wilson.) In the table, a '*' indicates the experiments which included UVP measurements of velocity, i.e. the three mixed sand

Table 2
Test conditions and measured maximum erosion depths, maximum sheet flow layer thicknesses and net sand transport rates

Experiment	T (s)	A (m)	u_{m} (m/s)	u_{rms} (m/s)	θ_{m}	δ_{em} (mm)	δ_{sm} (mm)	q_{N} (m^3/s/m)$\cdot 10^{-6}$
FA5010	5.0	1.0	1.53	0.89	3.9	5.1	16.9	−128
FA7515	7.5	1.5	1.53	0.89	3.6	4.2	10.9	−88
MA5010	5.0	1.0	1.53	0.89	2.4	3.6	8.2	53
MA7515	7.5	1.5	1.53	0.89	2.2	3.4	8.9	36
CA5010	5.0	1.0	1.53	0.89	1.5	3.8	6.1	44
CA7515	7.5	1.5	1.53	0.89	1.4	3.2	6.5	34
X1A5010*	5.0	1.0	1.53	0.89	3.2	4.4	12.4	15
X1A7515*	7.5	1.5	1.53	0.89	3.0	3.7	8.0	21
X2A5010*	5.0	1.0	1.53	0.89	2.4	3.9	10.4	46
X2A7515	7.5	1.5	1.53	0.89	2.2	4.8	11.6	32
X4A5010*	5.0	1.0	1.53	0.89	2.4	4.2	11.0	38
X4A7515*	7.5	1.5	1.53	0.89	2.2	4.4	11.4	22

beds (X1, X2, X4) in the 5-s flow and two of the mixed beds (X1, X4) in the 7.5-s flow. The UVP was not available when the other experiments were being carried out. Table 2 also presents the maximum erosion depths and sheet flow layer thicknesses based on the CCM concentration measurements as reported in O'Donoghue and Wright (2004).

5. Velocity results

Fig. 6 shows the measured velocity profiles at eight phases of the flow cycle (the phases are indicated in Fig. 5) and the time-averaged velocity profiles for (a) the Mix1, Mix2 and Mix4 sands in flow A5010 and (b) the Mix1 and Mix4 sands in flow A7515. The

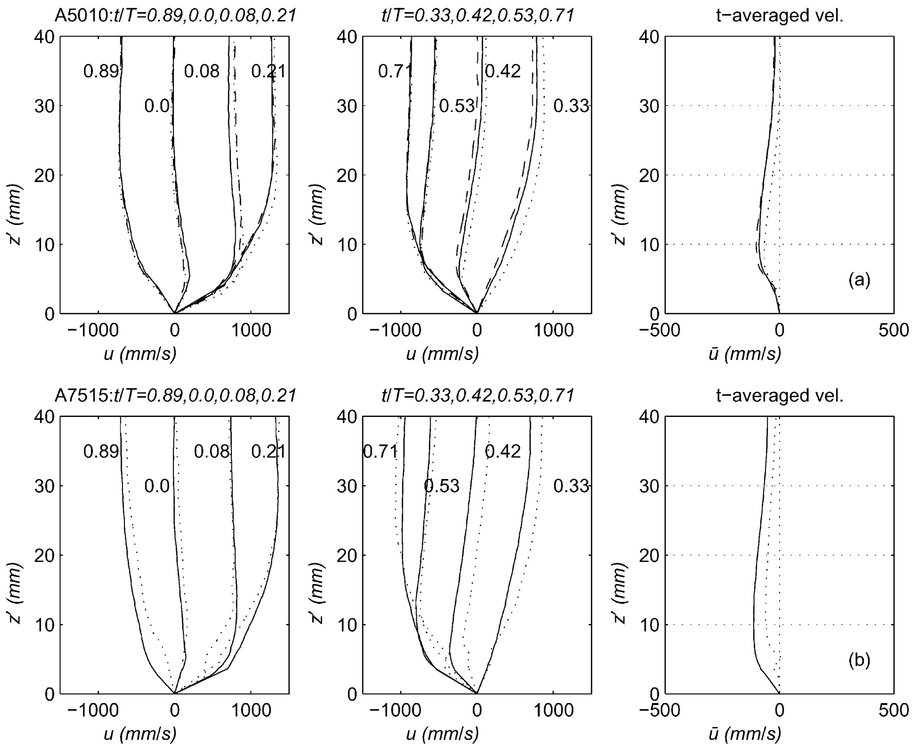

Fig. 6. Velocity profiles at selected phases and time-averaged velocity profiles. Top: flow A5010 and sand X1 (solid line), X2 (dashed), X4 (dotted). Bottom: flow A7515 and sand X1 (solid line) and X4 (dotted).

profiles are plotted with respect to the instantaneous erosion depth, i.e. u as a function of z', where $z'=z+\delta_e$. The UVP generally produced good measurements of velocity for $z\geq 0$ mm, i.e. down to the no-flow bed level. To extend the velocity profile to $z=-\delta_e$, a linear velocity profile was assumed between the UVP-measured u at $z\cong 0$ mm and $u=0$ at $z=-\delta_e$. The linear assumption is consistent with results from Dick and Sleath (1991, 1992) and Zala-Flores and Sleath (1998) for sheet flow velocity profile involving artificial sediments.

The profiles in Fig. 6 show two well known features of asymmetric oscillatory boundary layer flow: (i) a phase lead between flow in the boundary layer and the outer flow and (ii) a very low velocity, offshore-directed, near-bed net flow generated in the oscillatory boundary layer by asymmetry in near-bed turbulence between successive half-cycles of the flow (Davies and Li, 1997). The phase lead and decay in velocity amplitude as the bed is approached is shown in a different way in Fig. 7 in which velocity time-series at eight elevations for the five experiments are presented, extending from very close to the undisturbed bed to the outer flow. The phase lead is seen to be quite consistent across the experiments with an average value of 21.5°. (The time series in Fig. 7 consist of 100 points over the flow period, which implies an uncertainty of ±1.8° in the phase estimates.) As expected, this is much less than the theoretical 45° phase lead for laminar flow. It is similar to the 15–20° measured by Dick and Sleath (1991, 1992) and Zala-Flores and Sleath (1998) for sheet flow experiments with artificial sediments and the 24° phase lead that can be seen in the example result from flow tunnel experiments with sand shown by McLean et al. (2001).

Fig. 8 presents vertical profiles of u/u_m at $t/T=0.21$, i.e. at the phase corresponding to maximum onshore flow velocity, for each of the five experiments. With the exception of experiment X4A7515, the velocity profiles show a slight overshoot. The elevation of maximum velocity is shown for the cases with

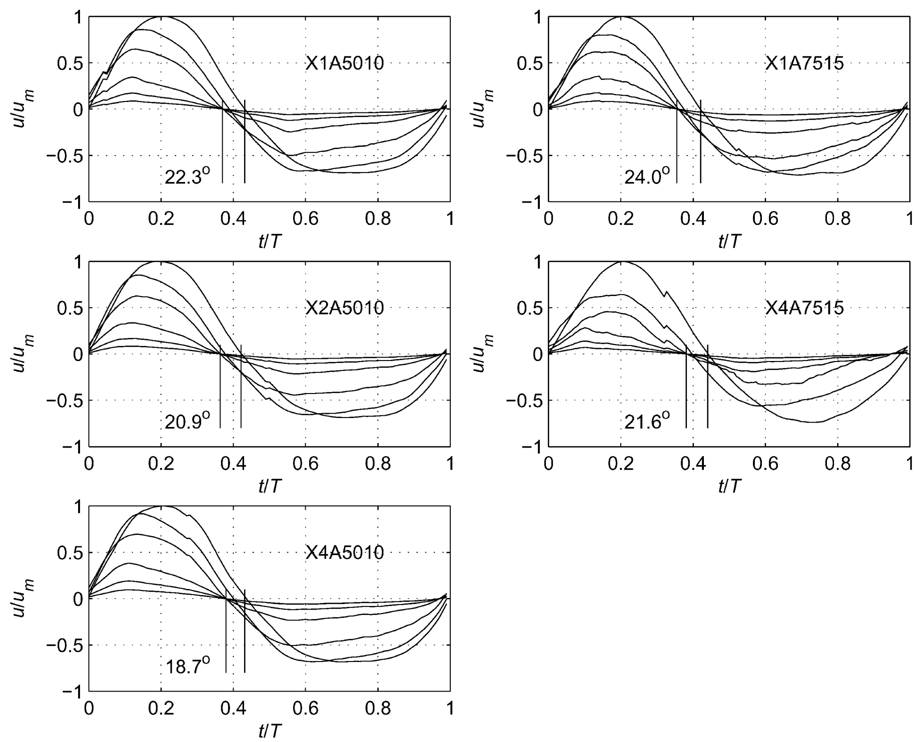

Fig. 7. Velocity time-series at z'=0.5, 1, 2, 5, 10 and 45 mm for each experiment.

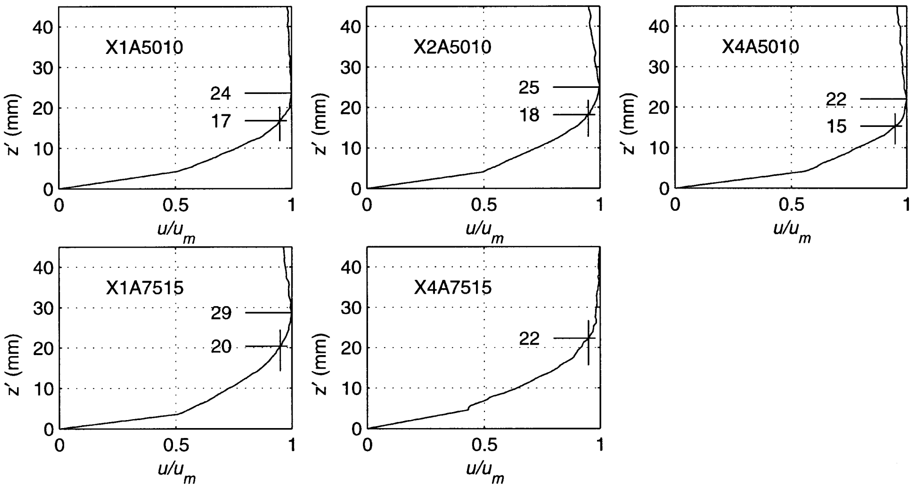

Fig. 8. Velocity profiles at phase t/T=0.21; numbers refer to elevations (mm) where u/u_m=0.95 and corresponding to maximum overshoot.

overshoot in Fig. 8 and the elevation on the profile where u/u_m=0.95 is shown for all five cases. Either of these elevations could be used as a measure of the boundary layer thickness, δ_b. Both are somewhat less than δ_b determined using Sleath's formula (Sleath, 1987) but the higher values, i.e. the values based on the elevation of the overshoot, are in good agreement with δ_b calculated using the following formula for fixed bed boundary layer presented by Fredsoe and Deigaard (1992):

$$\frac{\delta_b}{k_N} = 0.09\left(\frac{A}{k_N}\right)^{0.82} \tag{6}$$

The calculated values using Eq. (6) are 22, 24, 24 and 32 mm for experiments X1A5010 (measured 24 mm), X2A5010 (25 mm), X4A5010 (22 mm) and X1A7515 (29 mm), respectively. In the calculations, the roughness is taken as k_N=2.5d_{50}, rather than some multiple of the sheet flow layer thickness as suggested by some authors.

In Fig. 6, the velocity profiles for the same flow but different sand beds are seen to be similar. This is particularly true in the case of flow A5010. The results suggest that the near-bed velocities for a given main flow condition are not very sensitive to sand size and grading, at least for the size and grading range covered by the Mix1, Mix2 and Mix4 sands of the present study. On this basis, in order to obtain flux results for all 12 experiments, we assume that the mean of velocities measured in experiments X1A5010, X2A5010 and X4A5010 applies to experiments FA5010, MA5010 and CA5010 (for which no UVP measurements were made); similarly, we assume that the mean of velocities measured in experiments X1A7515 and X4A7515 applies to experiments FA7515, MA7515, CA7515 and X2A7515 (for which no UVP measurements were made).

6. Results for sand flux

The velocity measurements discussed above have been combined with the corresponding concentration measurements (discussed in detail in O'Donoghue and Wright, 2004) to produce estimates of time- and z-varying sand flux for all of the experiments listed in Table 2.

6.1. Time-varying sediment flux

Figs. 9 and 10 show example sediment flux profiles for the fine and medium sands respectively in flow A5010. Eight profiles are presented, corresponding to the phases indicated in Fig. 5. Fluxes in the sheet flow layer are based on CCM-measured concentrations and UVP-measured velocities; fluxes in the suspension layer are based on suction sampled concentrations and UVP-measured velocities. As described earlier, the CCM and suction measurements

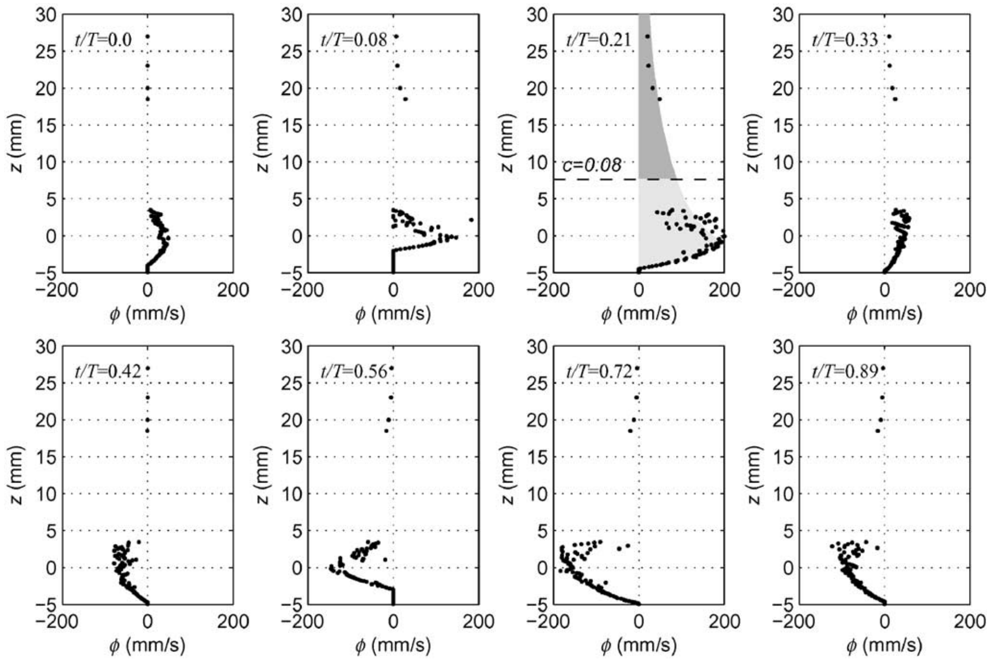

Fig. 9. Flux profiles at selected phases (Fig. 5) for experiment FA5010.

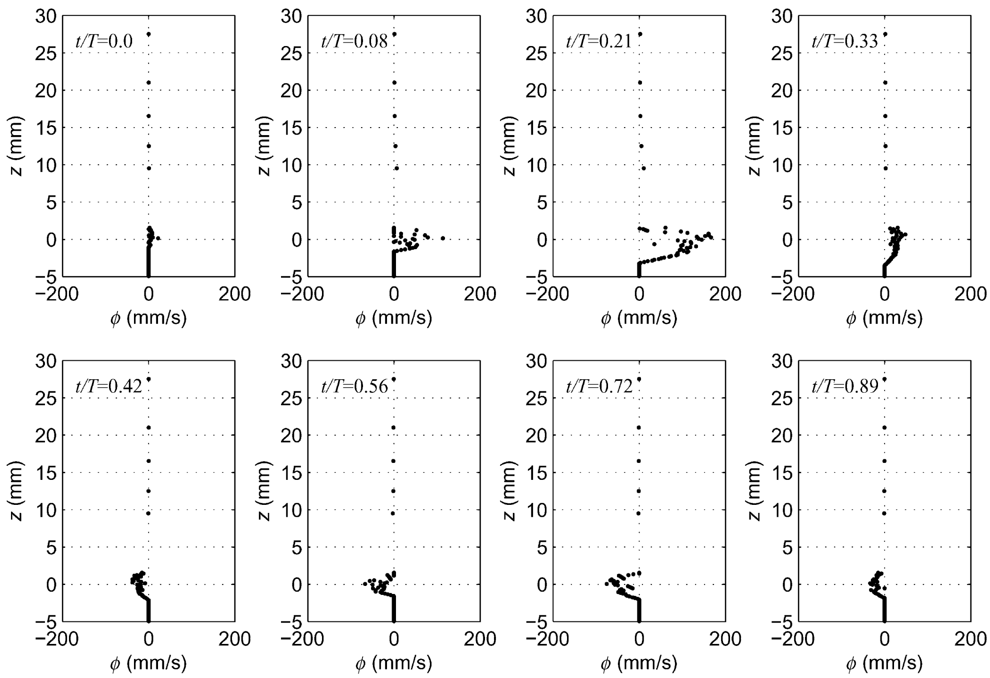

Fig. 10. Flux profiles at selected phases (Fig. 5) for experiment MA5010.

do not overlap, with the result that a 5–15-mm gap occurs in the flux profiles between the topmost CCM-based flux and the lowest suction-based flux. There is large scatter in the flux data towards the top of the sheet flow layer where small scatter in concentration data is multiplied by large velocities.

The following is noted from the example flux profiles shown in Figs. 9 and 10. (i) As expected, flux magnitudes are much greater in the case of the fine sand compared with the medium sand. This is due to the higher concentrations of sand in suspension in the case of the fine sand. (ii) For both sands, flux is highest in the sheet flow layer. In the case of the medium sand, flux is very small in the suspension layer, even at times of high flow velocity, because the medium sand entrained by the flow remains in close proximity to the bed. Flux in the suspension layer is more significant in the case of the fine sand, especially at times of high velocity when fine sand is carried high into the flow. The importance of the contribution of suspension layer flux to the overall flux in the case of the fine sand is illustrated by the flux profile at maximum onshore velocity (t/T=0.21) in Fig. 9. Here, we distinguish between the suspension and sheet flow layers using the 8% volumetric concentration criterion. The shaded areas in the figure show that, while the highest flux occurs in the sheet flow layer, the integrated flux at this phase comprises approximately equal contributions from the sheet flow and suspension layers. (iii) As expected, highest fluxes generally occur at times of high flow velocity. However, in the case of the fine sand, we see flux values at the time of maximum offshore velocity (t/T=0.72) that are as high as the flux values at the time of maximum onshore velocity (t/T=0.21), even though maximum offshore velocity is only approximately 60% of the maximum onshore velocity. The reason for this is the unsteady effects that occur in the case of fine sand, what Dohmen-Janssen et al. (2002) call the "phase lag effect". The phenomenon is summarised as follows. At t/T=0.21, fine sand is carried high into the flow as a result of the high flow velocities, contributing to high onshore flux at this phase. Because of its low settling velocity, this sand is slow to settle and a significant proportion does not settle back to the bed as the flow velocity decreases. A proportion is therefore available for transport in the offshore direction when the flow reverses. The high offshore flux during the offshore flow is therefore due to the presence of high sand concentrations resulting from the slow settling of sand entrained by the previous high onshore velocities.

6.2. Time-averaged sediment flux

While the time-dependent flux profiles hold all of the detailed behaviour, examination of integrated flux results reveals important aspects of the fundamental sediment transport processes. We start by looking at the time-averaged flux profile for one experiment. This leads to a generalised schematic illustrating fundamental differences between the time-averaged flux profiles for the different sands.

Time-averaged, z-varying flux is given by

$$\bar{\phi}(z) = \frac{1}{T}\int_0^T \phi(t,z)\mathrm{d}t \tag{7}$$

The time-averaged flux profile for the Mix2 sand in flow A7515 is shown in Fig. 11. Time-series of concentration, velocity and flux at five elevations in the flow—z=11.5, 1, 0, −2.5 and −3.5 mm—are also shown; these elevations correspond to the numbered arrows 1–5 on the flux profile. (Note the factor of 10, 50 or 100 difference in scale between the position 1 time series and the other time series.) The maximum erosion depth during the onshore (positive) flow is 4.7 mm, while the maximum erosion depth during the offshore (negative) flow is 3.1 mm; these are indicated by $\delta_{\mathrm{e(on)}}$ and $\delta_{\mathrm{e(off)}}$, respectively, in Fig. 11.

The following method was used to close the gap in the time-averaged flux profile caused by the gap between the CCM and suction concentration measurements. The net transport rate, q_{N}, is equal to the integral over the depth of the time-averaged flux. If the water depth is h, then

$$q_{\mathrm{N}} = \int_{z=-\delta_{\mathrm{e}}}^{z=h} \bar{\phi}(z)\mathrm{d}z = \underbrace{\int_{\mathrm{CCM}} \bar{\phi}(z)\mathrm{d}z}_{(I_1)} + \underbrace{\int_{\mathrm{suction}} \bar{\phi}(z)\mathrm{d}z}_{(I_2)} + \underbrace{\int_{\mathrm{gap}} \bar{\phi}(z)\mathrm{d}z}_{(I_3)} \tag{8}$$

Because q_{N} has been measured for each experiment (Table 2) and the integrals I_1 and I_2 can be

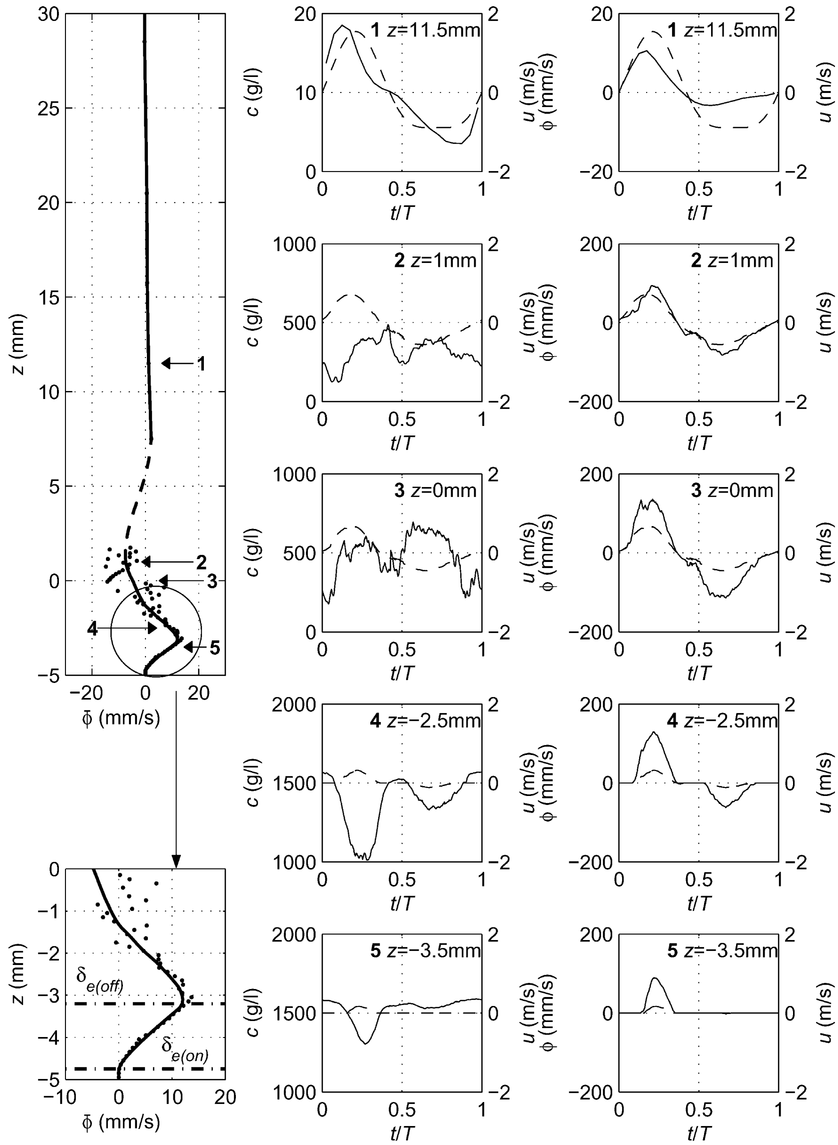

Fig. 11. Experiment X2A7515: time-averaged flux profile and time-series of velocities (dashed lines) and concentrations and fluxes (solid lines) at selected elevations.

determined from the CCM-based and suction-based flux data respectively, the integrated sediment flux in the gap, I_3, can be calculated. For each experiment, a cubic spline method was used to estimate the time-averaged flux profile in the gap such that the integrated flux in the gap equates to I_3. A broken line is used in Fig. 11 to indicate the resulting estimate of the time-averaged flux profile between the CCM-based and suction-based results.

The concentration, velocity and flux time-series shown in Fig. 11 for the five locations help to explain the time-averaged flux profile, as follows:

(i) $-\delta_{e(on)} \leq z \leq -\delta_{e(off)}$. The $c(t)$, $u(t)$ and $\phi(t)$ time-series shown for location 5, $z=-3.5$ mm illustrate what is happening in this region. Sand is only mobilised around the time of maximum onshore velocity and the flux is positive (onshore) at this time; the flux is zero at all other times. The time-averaged flux is therefore positive in this region and increases with increasing z above $\delta_{e(on)}$.

(ii) $z=-1$ mm corresponds to the top of the pick-up layer for this experiment. In the region $-\delta_{e(off)} \leq z \leq -1$ mm sand is mobilised during onshore and offshore flow, resulting in positive and negative flux during the flow cycle. Location 4 at $z=-2.5$ mm is just above $\delta_{e(off)}$, is therefore very close to the undisturbed bed level during the offshore half-cycle but is well above the undisturbed bed level during the onshore half-cycle. For this reason, we see higher velocities and lower concentrations during onshore flow compared to offshore flow. For location 4, the product of velocities and concentrations during the onshore flow produces higher fluxes than the product of lower velocities and higher concentrations during the offshore flow with the consequence that net flux is positive. For increasing z in this region, the magnitude of the negative flux increases relative to the magnitude of the positive flux with the result that net flux decreases with increasing z.

(iii) $z=5$ mm corresponds roughly to the top of the sheet flow layer for this experiment. The region $-1 \leq z \leq \sim 5$ mm corresponds to the upper sheet flow layer where concentrations tend towards being in phase with the outer flow velocity and high concentrations occur at times of maximum velocity. The concentration time-series therefore contain two peaks, roughly corresponding to velocity peaks in the two half-cycles. The phase lag effects described earlier lead to high concentrations occurring during the offshore flow and, coupled with the longer duration offshore flow, produce a negative net flux in this region.

(iv) $z>5$ mm corresponds to the suspension layer. Here, velocities are high as the top of the boundary layer is approached but concentrations are very low and flux magnitudes are consequently small, as illustrated by the $c(t)$, $u(t)$ and $\phi(t)$ time-series shown for location 1, $z=11.5$ mm. Time-averaged flux tends to be positive in the suspension layer, resulting from more sand being carried relatively high in the flow by the higher onshore (positive) velocities than by the lower offshore (negative) velocities. (It is the subsequent settling of this sand that contributes to the negative flux at lower elevations during the offshore flow.) The flux decays to zero for increasing z in the suspension layer because of the decay in concentration with increasing z.

Time-averaged sediment flux profiles for all 12 experiments are shown in Fig. 12. (In Fig. 12, the dashed line in each graph marks the elevation in the flow where the time-averaged concentration is 8%.) The profiles depend strongly on sediment size and this is illustrated schematically in Fig. 13. Profile 1 in Fig. 13 characterises the time-averaged flux profile that occurs in cases of fine sand. In such cases, the erosion depth tends to be less dynamic than for coarser sands so that $\delta_{e(on)} \approx \delta_{e(off)}$, strong unsteady effects lead to a high negative time-averaged flux in a relatively thick sheet flow layer and onshore time-averaged flux in the suspension layer extends to a relatively large height above the bed. The time-averaged flux profiles for the fine sand (FA5010 and FA7515) and the fine-dominated Mix1 sand in Fig. 12 (X1A5010 and X1A7515) essentially follow profile type 1. Profile 3 in Fig. 13 characterises the time-averaged flux profile that occurs in cases of coarse sand. In such cases, the maximum erosion depth during the higher velocity onshore flow is significantly greater than the maximum erosion depth during offshore flow. This leads to a strong onshore time-averaged flux at the base of the sheet flow layer. Because of its high settling velocity, coarse sand stays close to the bed during the flow and sand that is entrained at times of high velocity settles back to the bed as the flow velocity decreases. Profile type 3 is therefore contained within a thin layer close to the bed and is directed onshore (positive). The time-averaged flux profiles for the coarse sand in Fig. 12 (CA5010 and CA7515) essentially follow profile type 3.

Profile 2 in Fig. 13 characterises the time-averaged flux profile that occurs in cases of medium sands. It contains features of profile types 1 and 3: there is positive flux in the lower sheet flow layer, negative flux in the upper sheet flow layer and positive flux in the suspension region. The time-averaged flux profiles for the medium sand (MA5010 and MA7515), the Mix2 sand (X2A5010 and X2A7515) and the Mix4

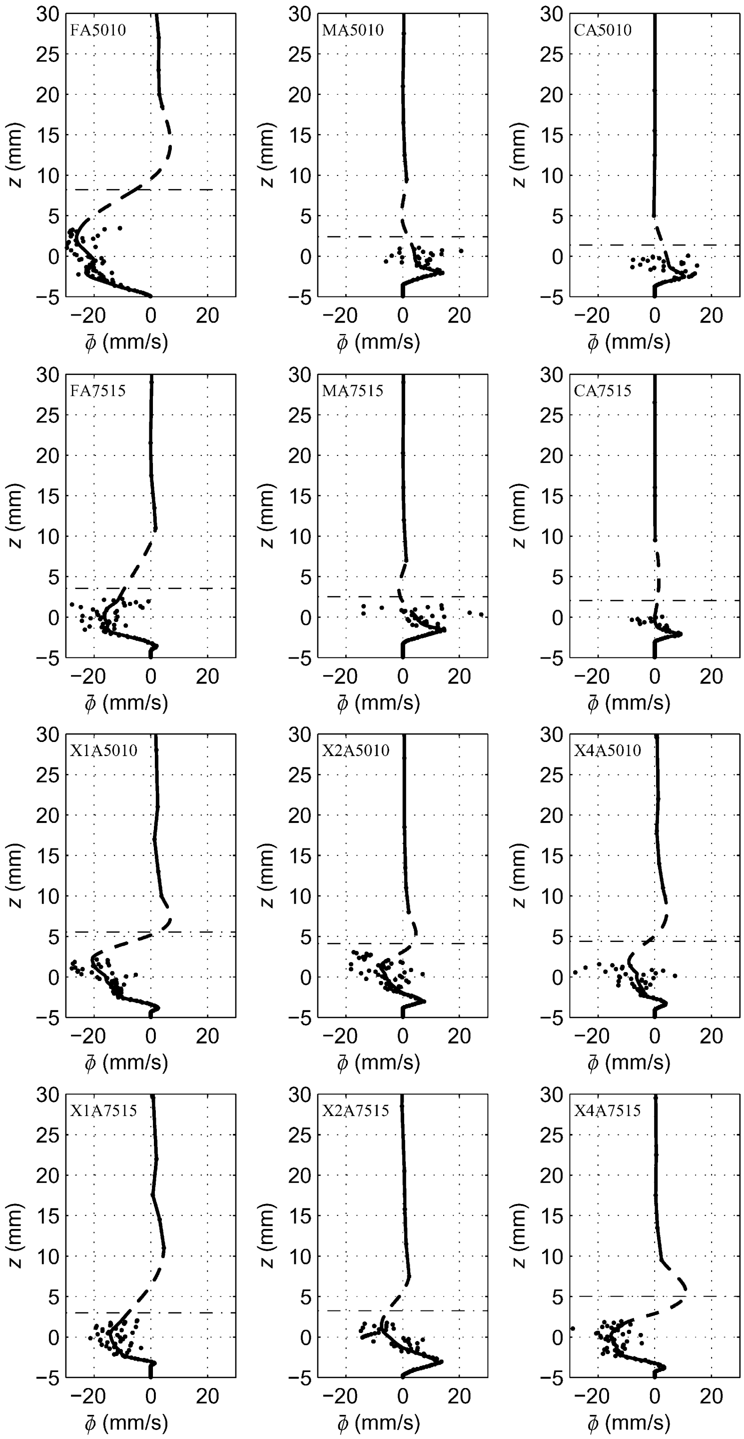

Fig. 12. Time-averaged flux profiles for all 12 experiments.

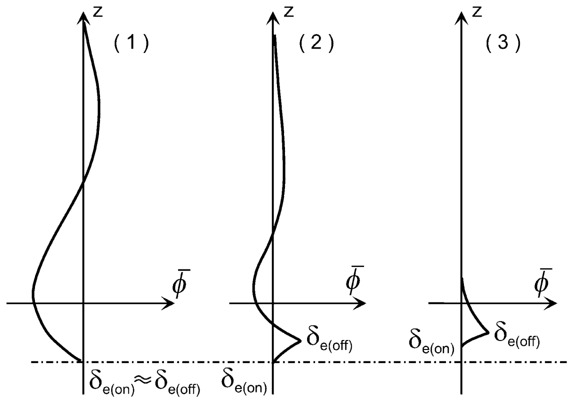

Fig. 13. Generalised time-averaged flux profiles.

sand (X4A5010 and X4A7515) essentially follow profile type 2, but the relative dominance of particular features of the profile varies considerably across these sands, despite the fact that they have the same d_{50}. For example, the Mix2 profiles (X2A5010 and X2A7515) are very close to profile type 2, the medium profiles (MA5010 and MA7515) show a strong tendency towards profile type 3 and the Mix4 profiles (X4A5010 and X4A7515) show a strong tendency towards profile type 1. The reason for this is the difference in grading between the sands: the greater the percentage of fine sand, the greater the unsteady effects and the more the profile tends towards profile type 1, with increased negative flux in the sheet flow layer and increased onshore flux in the suspension layer. The net effect is a decrease in onshore net sand transport with increasing % of fine sand in the bed, as seen in the measured net transport results presented in Table 2.

6.3. Onshore and offshore sand transport

Integrating the positive and negative flux regions of the time-averaged sediment flux profile gives the onshore (q_{on}) and offshore (q_{off}) net transport rates, respectively,

$$q_{on} = \int \bar{\phi}_{+}(z)dz \quad \text{and} \quad q_{off} = \int \bar{\phi}_{-}(z)dz \qquad (9)$$

where ϕ_{+} and ϕ_{-} are onshore (positive) and offshore (negative) flux, respectively. The results are presented in Fig. 14, where the open and solid symbols represent onshore and offshore transport rates respectively and the crosses indicate the net transport rate, q_N=q_{on}+q_{off}. A broken line links the medium, Mix2 and Mix4 q_N values in Fig. 14 because these sands have the same d_{50}.

Transport in the case of the coarse sand is totally onshore (refer to profile 3 in Fig. 13) and is almost totally onshore in the case of the medium sand. Onshore and offshore transport rates generally increase as the sand becomes finer (smaller d_{50}) and as the percentage of fine sand in the bed increases. Broadly speaking, the increase in onshore transport corresponds to an increase in onshore transport in the suspension region and the increase in offshore transport corresponds to an increase in offshore transport in

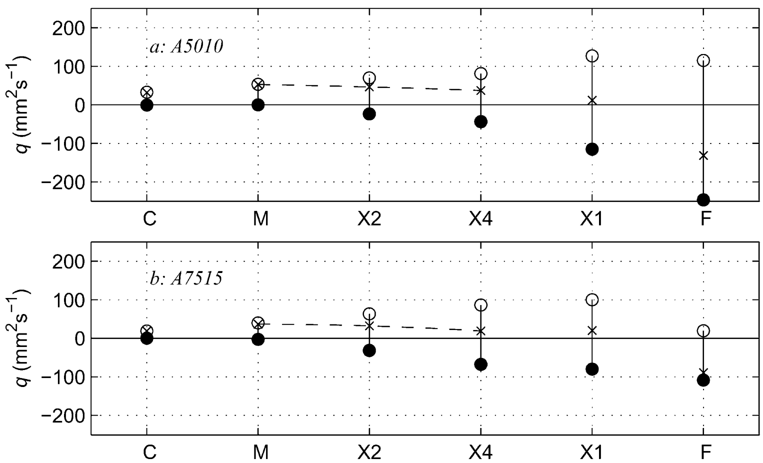

Fig. 14. Offshore (solid circles) and onshore (open circles) transport rates for (a) flow A5010 and (b) flow A7515.

the sheet flow layer resulting from the increase in unsteady phase lag effects. The increase in offshore transport is greater than the increase in onshore transport with the result that the net transport (q_N) decreases and becomes strongly negative as the sand goes from medium to fine in Fig. 14.

High negative (offshore) transport in the case of fine sand has also been observed in the LOWT experiments of Ribberink and Chen (1993), which involved asymmetric oscillatory flow and a 0.13-mm sand similar to the fine sand used in the present experiments. The negative net transport and the reduction in net transport with increasing percentage of fine sand in the bed are a result of unsteady phase lag effects that are fundamentally important in the context of predictive formulae for sand transport in sheet flow conditions, as discussed by Dohmen-Janssen et al. (2002). Commonly used transport formulae are quasi-steady in the sense that the instantaneous transport rate is related to the instantaneous velocity through the instantaneous Shields parameter (Bailard, 1981; Ribberink, 1998). For asymmetric flows of the type considered here, these formulae will always lead to an onshore net transport, which increases with decreasing sand size. This is at odds with the experimental results for fine sands, which show a decreasing and ultimately offshore net transport as the percentage of fine sand in the bed increases. The "semi-unsteady" model recently proposed by Dohmen-Janssen et al. (2002) aims to account for unsteady effects by applying a correction factor, r, to Ribberink's (1998) quasi-steady transport formula. r depends on a phase lag parameter and $0<r<1$, which means that it acts to reduce the transport rates but does not lead to the high negative net transport rates measured in the experiments. The detailed flux results presented in this paper can contribute towards improving these semi-unsteady predictive models.

6.4. Sand transport in the sheet flow and suspension layers

It is often assumed that under sheet flow conditions the bulk of the transport takes place within the sheet flow layer. However, it is clear from Fig. 12 that for many experiments a substantial contribution to the net transport comes from the suspension layer. The actual relative contributions can be estimated from the time-averaged flux profiles. The net transport rates in the sheet flow layer and in the suspension region are estimated from

$$q_{sf} = \int_{z=-\delta_e}^{z=z_s} \bar{\phi}(z)\mathrm{d}z \quad \text{and} \quad \mathrm{q_{sp}} = \int_{z=z_s}^{z=h} \bar{\phi}(z)\mathrm{d}z \tag{10}$$

respectively, where z_s corresponds to the top of the sheet flow layer. For the present purposes, z_s is taken as the elevation where the time-averaged concentration is 8% and is indicated by the broken line in each graph of Fig. 12. The calculated net transport rates for the two regions are presented in Fig. 15: the solid

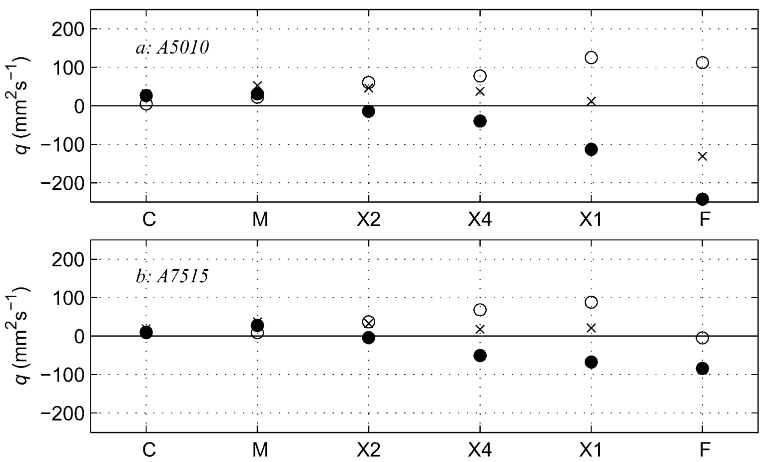

Fig. 15. Net transport rate in the sheet flow (solid circles) and suspended (open circles) regions for (a) flow A5010 and (b) A7515.

circles correspond to the sheet flow net transport, the open circles correspond to the suspension net transport and, as in Fig. 14, the crosses indicate the net transport, $q_N = q_{sf} + q_{sp}$. Note that it is the net transport rate in each of the two regions that is presented in Fig. 15, not the total transport rate (equal to $|q_{on}| + |q_{off}|$ for the region); the total transport in each region is generally greater than the net transport because the sheet flow layer and the suspension region both contain regions of onshore and offshore time-averaged flux.

In general, net transport in the suspension layer is directed onshore and increases as the percentage of fine sand in the bed increases. The exceptions are the cases of coarse sand, for which suspended transport is negligible, and fine sand in flow A7515 (FA7515), for which onshore transport occurring high in the suspension region is cancelled by offshore transport occurring at the bottom of the suspension region. Net transport in the sheet flow layer is directed onshore for the coarse and medium sands and is offshore for the fine and mixed sands. The reasons for this have already been discussed. The relative magnitudes of net sheet flow and net suspension transport varies across the six sands: sheet flow transport dominates in the case of the coarse, medium and fine sands, while suspended transport dominates in the case of the mixed sands but this conclusion is sensitive to the definition used for the sheet flow/suspension boundary (i.e. the elevation of the broken line in each graph of Fig. 12).

6.5. Time-varying sand transport in the sheet flow layer

Time-varying sediment transport is obtained by integrating the instantaneous flux profile, i.e.

$$\hat{\phi}(t) = \int \phi(t,z)\mathrm{d}z \tag{11}$$

While the gap in the time-averaged flux profile between the CCM-based results and the suction-based

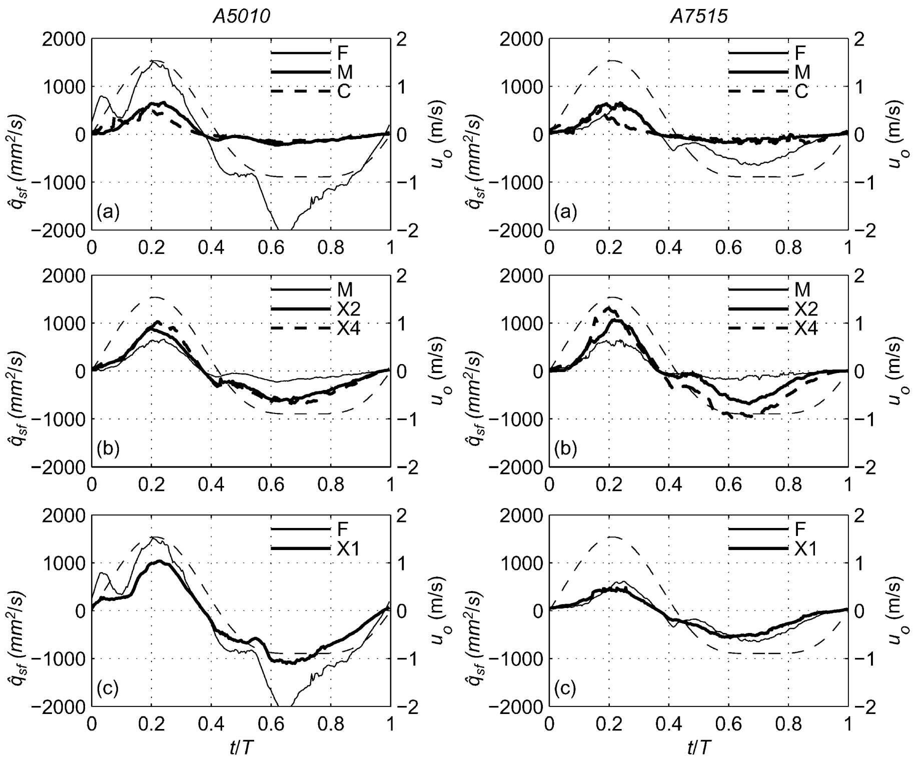

Fig. 16. Time-dependent (phase-averaged) transport in the sheet flow layer. Top panels: comparison of $\hat{q}_{sf}$ for F, M and C sands. Middle panels: comparison for M, X2 and X4 sands. Bottom panels: comparison for F and X1 sands.

results can be estimated using the measured net transport, it is not possible to bridge the gap in the case of the time-varying flux profiles. However, the CCM-based data extends across the sheet flow layer, which makes it possible to examine time-varying transport in the sheet flow layer for each experiment. The time-varying sheet flow sediment transport is given by

$$\hat{\phi}_{\mathrm{sf}}(t) = \int_{z=-\delta_{\mathrm{e}}(t)}^{z=z_{\mathrm{s}}(t)} \phi(t,z)\mathrm{d}z \tag{12}$$

where $z_s(t)$ is the time-varying top of the sheet flow layer defined using the 8% criterion. Time-series of sheet flow transport are presented for all 12 experiments in Fig. 16. The results are grouped (a) to compare sheet flow transport for the fine, medium and coarse sands; (b) to compare sheet flow transport for the medium, Mix2 and Mix4 sands; and (c) to compare sheet flow transport for the fine and Mix1 (fine-dominated) sands. The broken line in each graph of Fig. 16 indicates the outer flow velocity. The results presented in Fig. 16 echo earlier observations. Sheet flow transport is much more dynamic in the case of the fine sand compared to the coarse and medium sands, in the sense that the fine sand exhibits much larger positive and negative transport rates with high negative transport caused by the strong unsteady effects being especially significant. Mix1 contains 60% of the fine sand and has a d_{50} that is a little greater than that of the fine sand. Sheet flow transport for Mix1 follows that of the fine sand quite closely but is a little less dynamic because of its larger size. Grading effects, and in particular the effects of increased percentage of fine sand in the bed, are seen in the results for the medium, Mix2 and Mix4 sands. These sands have the same d_{50} but contain different percentages of fine sand. The fine sand fraction in Mix2 and Mix4 leads to an increase in positive sheet flow transport during the onshore flow and a large increase in negative transport during the offshore flow. Again, this can be attributed to the increased unsteady effects as discussed earlier. As seen earlier in Fig. 15, net sheet flow transport goes from being onshore-dominant in the case of the medium sand to being offshore-dominant in the case of the Mix2 and Mix4 sands.

7. Conclusions

New data for sheet flow velocities and sheet flow fluxes have been obtained from large-scale flow tunnel experiments involving well-sorted and mixed sands in asymmetric oscillatory flows. The main conclusions are summarised as follows:

(1) Velocity profiles measured over the mobile sand beds show well-known features of oscillatory boundary layer flow. The near-bed velocity leads the main flow velocity by approximately 21° and a small offshore-directed current (near-bed streaming) is produced near the bed by the asymmetry in turbulence generation. Measures of the boundary layer thickness are in good agreement with thicknesses calculated using a formula for fixed bed conditions presented by Fredsoe and Deigaard (1992).

(2) Time-averaged flux profiles are very different for sands of different size and grading. Time-averaged flux is onshore-directed (positive) in the case of coarse sand and is confined to a region immediately above the bed. In contrast, time-averaged flux in the case of fine sand extends high above the bed, is offshore-directed (negative) in the sheet flow layer and becomes onshore-directed in the suspension layer.

(3) Unsteady effects, which are dominant in the case of fine sand and largely absent in the case of coarse sand, explain the differences between the flux profiles for the fine and coarse sands. The unsteadiness arises because fine sand entrained under high velocities is carried high off the bed, is slow to fall back to the bed as the flow velocity decreases and is therefore available for transport in the opposite direction after flow reversal.

(4) Onshore, offshore and net transport depend on sand size and grading. Net transport in the case of coarse sand is directed onshore. Both onshore and offshore transport rates increase with increasing percentage of fine sand in the bed; the offshore transport becomes increasingly dominant however, with the result that the net transport decreases and ultimately becomes offshore-directed (negative).

(5) Net transport in the suspension layer is onshore but net transport in the sheet-flow layer may be onshore or offshore depending on sand size and grading. It is onshore in the case of coarse sand and offshore in the case of fine sand.

Finally, oscillatory flow tunnels provide an approximation to the flow experienced at the seabed under real waves. Phase differences in wave orbital motion, vertical orbital motions, wave-induced boundary layer streaming and undertow are not reproduced in flow tunnels. The impact of these differences on sheet flow processes and transport rates can only be measured through experiments carried out in a full-scale wave flume. Dohmen-Janssen and Hanes (2002) carried out sheet flow experiments in the 300-m long wave flume at Hannover (GWK, Hannover) and concluded that sheet flow processes under progressive waves are very similar to sheet flow processes in oscillatory flow tunnels. However, their results suggest that net transport rates under progressive waves may be up to 2.5 times the transport rates in "equivalent" flow tunnel oscillatory flow and they attribute the difference to the onshore-directed boundary layer streaming that is present under progressive waves but is not present in tunnel flow. Further measurements of sheet flow transport and processes under progressive waves are needed to establish better understanding of these effects. Despite potentially significant differences between net sand transport rates in oscillatory flow tunnel flows and under progressive waves, detailed flow tunnel experimental results of the kind presented in this paper are important for improving understanding and developing predictive models for sand transport in sheet flow conditions.

Acknowledgements

The research was carried out with funding from the UK Engineering and Physical Sciences Research Council (EPSRC Grants GR/M75563, GR/R23572). Thanks to Rab Fraser and other technical staff in the Department of Engineering at Aberdeen for assistance with the laboratory work and to Malcolm Sunter for his work on some of the figures. The Malvern particle size analyser was borrowed from the EPSRC Equipment Loan Pool.

Appendix A

Notation

A amplitude of outer flow horizontal excursion
as asymmetry in outer flow horizontal velocity
C_1, C_2 empirical constants
c sediment concentration
c_o sediment concentration in undisturbed bed (1600 g/l)
c' normalised concentration, c/c_o
$\bar{c}$ time-averaged concentration
d sediment size
d_{10}, d_{50}, d_{90} size for which 10%, 50%, 90% of the sediment sample is finer
f_w friction factor
g acceleration due to gravity
k roughness height
q_N net sand transport rate
q_{on}, q_{off} net onshore, offshore sand transport rate
q_{sf}, q_{sp} net sheet flow, suspension sand transport rate
s sediment-specific gravity
t time
T flow period
u flow velocity in boundary layer
u_o outer flow velocity
u_m, u_{min} maximum, minimum outer flow velocity
u_{rms} root mean square outer flow velocity
z vertical coordinate relative to undisturbed bed level
z' vertical coordinate relative to erosion depth, $z'=z+\delta_e$
δ_e, δ_{em} erosion depth, maximum erosion depth
δ_s, δ_{sm} sheet flow layer thickness, maximum sheet flow layer thickness
δ_b boundary layer thickness
ϕ sand flux
$\bar{\phi}$ time-averaged, z-varying flux
$\hat{\phi}$ z-averaged, phase-averaged sand flux
$\hat{\phi}_{sf}$ z-averaged, phase-averaged sand flux in the sheet flow layer
θ, θ_m Shields parameter, maximum value of Shields parameter

ρ water density
τ_o, τ_{om} bed shear stress, maximum value of bed shear stress
ω flow angular frequency ($2\pi/T$).

References

wAsano, T., 1992. Observations of granular-fluid mixture under an oscillatory sheet flow. ASCE, Proceedings 23rd International Conference on Coastal Engineering, pp. 1896–1909.

Asano, T., 1995. Sediment transport under sheet flow conditions. ASCE Journal of Waterway, Port, Coastal and Ocean Engineering 121 (5), 239–246.

Bailard, J.A., 1981. An energetics total load sediment transport model for a plane sloping beach. Journal of Geophysical Research 86, 10938–10954.

Bosman, J.J., Van der Velden, E.T.J.M., Hulsbergen, C.H., 1987. Sediment concentration measurement by transverse suction. Coastal Engineering 11, 353–370.

Davies, A.G., Li, Z., 1997. Modelling sediment transport beneath regular symmetrical and asymmetrical waves above a plane bed. Continental Shelf Research 17 (5), 555–582.

Dibajnia, M., Watanabe, A., 1991. Sheet flow under nonlinear waves and currents. ASCE, Proceedings 23rd International Conference on Coastal Engineering, Venice, pp. 2015–2028.

Dibajnia, M., Watanabe, A., 1998. Transport rate under irregular sheet flow conditions. Coastal Engineering 35, 167–183.

Dick, J.E., Sleath, J.F.A., 1991. Velocities and concentrations in oscillatory flow over beds of sediment. Journal of Fluid Mechanics 233, 165–196.

Dick, J.E., Sleath, J.F.A., 1992. Sediment transport in oscillatory sheet flow. Journal of Geophysical Research 97, 5745–5758.

Dohmen-Janssen, C.M., 1999. Grain size influence on sediment transport in oscillatory sheet flow: phase lags and mobile bed effects. PhD thesis, Delft University of Technology.

Dohmen-Janssen, C.M., Hanes, D.M., 2002. Sheet flow dynamics under monochromatic non-breaking waves. Journal of Geophysical Research-Oceans 107 (C10), 13-1–13-21 (art.no.3149).

Dohmen-Janssen, C.M., Kroekenstoel, D.F., Hassan, W.N., Ribberink, J.S., 2002. Phase lags in oscillatory sheet flow: experiments and bed load modelling. Coastal Engineering 46, 61–87.

Dong, P., Zhang, K., 2002. Intense near-bed sediment motions in waves and currents. Coastal Engineering 45, 75–87.

Grant, W.D., Madsen, O.S., 1982. Movable bed roughness in unsteady oscillatory flow. Journal of Geophysical Research 87 (C1), 469–481.

Horikawa, K., Watanabe, A., Katori, S., 1982. Sediment transport under sheet flow condition. ASCE, Proceedings 19th International Conference on Coastal Engineering, pp. 1335–1352.

Jensen, B.L., Sumer, B.M., Fredsoe, J., 1989. Turbulent oscillatory boundary layers at high Reynolds number. Journal of Fluid Mechanics 206, 265–297.

Jonsson, I.G., 1966. Wave boundary layers and friction factors. ASCE, Proceedings 10th International Conference on Coastal Engineering, pp. 127–148.

Kaczmarek, L.M., Ostrowski, R., 2002. Modelling intensive near-bed sand transport under wave-current flow versus laboratory and field data. Coastal Engineering 45, 1–18.

Katopodi, I., Ribberink, J.S., Roul, P., Lodahl, C., 1994. Sediment transport measurements in combined wave-current flows. ASCE, Proceedings Coastal Dynamics '94, Barcelona, pp. 837–851.

Li, Z., Davies, A.G., 1996. Towards predicting sediment transport in combined wave-current flow. ASCE Journal of Waterway, Port, Coastal and Ocean Engineering 122 (4), 157–164.

McLean, S.R., Ribberink, J.S., Dohmen-Janssen, C.M., Hassan, W.N., 2001. Sand transport in oscillatory sheet flow with mean current. ASCE Journal of Waterway, Port, Coastal and Ocean Engineering 127 (3), 141–151.

Nielsen, P., 1992. Coastal bottom boundary layers and sediment transport. Advanced Series on Ocean Engineering, vol. 4. World Scientific, Singapore, ISBN: 981-02-0472-8.

O'Donoghue, T., Wright, S., 2004. Concentrations in oscillatory sheet flow for well sorted and graded sands. Coastal Engineering 50 (3), 117–138.

Ribberink, J.S., 1998. Bed-load transport for steady flows and unsteady oscillatory flows. Coastal Engineering 34, 59–82.

Ribberink, J.S., Al-Salem, A.A., 1994. Sediment transport in oscillatory boundary layers in cases of rippled beds and sheet flow. Journal of Geophysical Research 99, 12707–12727.

Ribberink, J.S., Al-Salem, A.A., 1995. Sheet flow and suspension of sand in oscillatory boundary layers. Coastal Engineering 25, 205–225.

Ribberink, J.S., Chen, Z., 1993. Sediment transport of fine sand under asymmetric oscillatory flow. Delft Hydraulics Report H840, part VII.

Sleath, J.F.A., 1987. Turbulent oscillatory flow over rough beds. Journal of Fluid Mechanics 182, 369–409.

Staub, C., Jonsson, I.G., Svendsen, I.A., 1996. Sediment suspension in oscillatory flow: measurements of instantaneous concentration at high shear. Coastal Engineering 27, 67–96.

Swart, D.H., 1974. Offshore sediment transport and equilibrium beach profiles. Publication-Delft Hydraulics Laboratory, vol. 131. Delft Hydraulics, The Netherlands.

Wilson, K.C., 1989. Friction of wave-induced sheet flow. Coastal Engineering 12 (4), 371–379.

Wilson, K.C., Andersen, J.S., Shaw, J.K., 1995. Effects of wave asymmetry on sheet flow. Coastal Engineering 25, 191–204.

Wright, S., 2002. Well-sorted and Graded Sands in Oscillatory Sheet-flow PhD Thesis, University of Aberdeen.

Zala-Flores, N., Sleath, J.F.A., 1998. Mobile layer in oscillatory sheet flow. Journal of Geophysical Research 103 (C6), 12783–12793.